Applied Clay Science 111 (2015) 50–60

Contents lists available at ScienceDirect

Applied Clay Science

journal homepage: www.elsevier.com/locate/clay

Research paper

Pore scale characterization of lime-treated sand–bentonite mixtures

M.A. Hashemi [a], T.J. Massart [a], S. Salager [b], G. Herrier [c], B. François [a,*]

[a] Building Architecture and Town Planning Department (BATir), Université Libre de Bruxelles, Avenue F.D. Roosevelt 50, CP 194/2, 1050 Brussels, Belgium
[b] CNRS UMR 5521, 3SR Lab, Grenoble-INP, UJF-Grenoble 1, 38041 Grenoble, France
[c] Lhoist Recherche et Développement S.A., rue de l'Industrie 31, 1400 Nivelles, Belgium

ARTICLE INFO

Article history:
Received 27 October 2014
Received in revised form 11 February 2015
Accepted 1 April 2015
Available online xxxx

Keywords:
Lime stabilization
Sand–bentonite mixture
X-Ray Tomography
Mercury Intrusion Porosimetry
Micro-scale analysis

ABSTRACT

Lime treatment of soils is a complex process which combines chemical and mechanical aspects of the soil behavior. The investigation presented here aims at understanding the effect of lime treatment of clayey soils by characterizing their microstructure evolution, along curing time, using X-Ray Micro-Computed Tomography (XRμCT) and Mercury Intrusion Porosimetry (MIP). Binary sand–bentonite mixtures are considered as a model material to simplify the soil microstructure and the diversity of phenomena involved in lime treatment. Samples containing 10%, 15% and 20% of bentonite and, respectively 90%, 85% and 80% of sand have been treated with 1% lime and compacted. Results in XRμCT show first that porosity is present at two scales: micropores within the bentonite aggregates and macropores between sand particles and bentonite aggregates. Micropores are shown to be exclusively saturated with water, while macropores are only full of air. Second, XRμCT images on the same sample at different curing times show the migration of lime enriched aggregates diffusing into bentonite during the first weeks of curing. Third, bentonite is shown to shrink progressively and to form clusters around the sand grains. Consequently, the fraction of macropores increases while the micropore size decreases. On the other hand, through MIP, three pore size categories have been determined: micropores, mesopores and macropores. The evolution in time of the three pore size categories seen in MIP confirms the behavior observed by XRμCT.

1. Introduction

Lime treatment of soils is widely used in civil engineering in order to increase the soil mechanical properties such as improved cohesion levels and load bearing capacities. Lime, calcium oxide or hydroxide, is an industrial mineral coming from the decarbonation process of calcium carbonate rocks by heating. Silty and clayey soils can be improved by the addition of small percentages of lime (Little, 1964). The advantage of this treatment lies in the low quantity of lime added and the potential related ecological advantages obtained by improving the properties of the soil already in place without requiring replacement. Lime treatment influences the soil behavior on two different time scales. First, lime quickly reacts with clay by modifying its structure, and allowing the clay minerals to merge to form larger aggregates (Little, 1964). Lime modification improves the soil towards a higher load-bearing capacity, a lower plasticity and a shift towards higher grain size distributions. The second effect is soil stabilization owing to the fact that long term pozzolanic reactions also take place after soil modification (Eades et al., 1962). Mineral formations obtained from pozzolanic reactions indeed confer relevant soil mechanical properties such as a higher cohesion level (Thompson, 1965), higher compressive/tensile strengths and frost resistance (Arabi et al., 1989). In lime-treated clayey soils, such reactions take place between the calcium of the lime and the silicates and aluminates of the clay minerals; and CSH (calcium silicate hydrate), CAH (calcium aluminate hydrate) and CASH (calcium aluminium silicate hydrate) are formed (Diamond and Kinter, 1965). However, the reaction kinetics is slow because it requires the dissolution of clay minerals into silicate and aluminate species and this dissolution is only possible for highly alkaline solutions (pH > 10) (Keller, 1964). Research on soil stabilization has been active during the last decades. Bell (1996), De Bel et al. (2009), Diamond and Kinter (1965) and many others observed an increase of the unconfined compressive strength (UCS) in lime-treated soils as a function of time. Many important parameters influence soil stabilization, such as the water content and the dry density of soil (Locat et al., 1990). Also, higher temperatures increase the speed of the reaction (De Bel et al., 2009), whereas the presence of organic matter could decrease the efficiency of lime (Locat et al., 1990). In addition, the clay mineral type is an important parameter of soil stabilization. Montmorillonite, for example, has a better efficiency for lime adsorption than kaolinite (Carroll, 1959), illustrating the importance to consider the cation exchange capacity (CEC) in the assessment of lime treatment.

In order to build a progressive understanding of lime treatment, this study aims at characterizing its influence on the microstructure of soils. This contribution combines MIP and XRμCT techniques in order to investigate the time dependent microstructural evolutions in lime-treated sand–bentonite controlled mixtures. The combination of these

* Corresponding author.
E-mail address: Bertrand.Francois@ulb.ac.be (B. François).

http://dx.doi.org/10.1016/j.clay.2015.04.001
0169-1317/

tools provides a visual interpretation with XRμCT as well as the quantitative MIP results on the micro-scale, and thereby sheds light on the microstructure development linked to lime treatment of soils. This study also clarifies the reorganization of a soil composed of a lime-reactive fraction (bentonite) and a non-reactive fraction (sand), as well as the influence of their proportion on the kinetics of the evolution and in the formation of a more or less cohesive matrix after lime-treatment. Let us mention that other methods can also be suggested to study microscale changes in lime-treated soils such as X-Ray Diffraction, Thermogravimetric Analysis and Transmission and Scanning Electron Microscopy, see Al-Mukhtar et al. (2012) for a review.

X-Ray Computed Tomography made its way to geosciences in the past decade for which a wide range of issues can be addressed. Its implementation is based on the computer processing of numerous snapshots of the sample taken at different angles by an X-Ray source. Since X-Rays pass through matter with a level of absorption that depends on the local density and atomic number, the snapshots represent the local X-Ray absorptivities of the sample. Computer processing allows further recombining the snapshots to form the entire 3D reconstruction of the object. A review for the use of XRμCT in geosciences can be found in works by Mees et al. (2003), Ketcham and Carlson (2011) and Desrues et al. (2006). Tomography carries the main advantage that the micro-fabric of materials is not disturbed by the observation technique, and was therefore used for various characterizations in a geomechanical context, in which the evaluation of densities, water content and volume fractions at small scale is of particular interest (Anderson et al., 1988; Taud et al., 2005; Riedel et al., 2012). Also, it is a powerful tool in order to follow local deformations as performed in Lenoir et al. (2007) for rock materials and Desrues et al. (1996) as well as Hall et al. (2010) and Higo et al. (2011) for sandy soils. Investigations on bentonite-based mixtures were also studied recently. In Kawaragi et al. (2009), the microstructure of sand–bentonite mixtures was analyzed through XRμCT for permeability studies for sealing plugs of radioactive waste disposal. In Saba et al. (2014), XRμCT was used to understand the effect of swelling non-homogeneities of a sand–bentonite mixture throughout the sample. Lime treatment investigation with XRμCT was recently carried out by Lemaire et al. (2013). Results show that lime binders aggregate the silt particles during short term soil modification and form a strong shell structure surrounding the aggregates during the long term soil stabilization. This shell structure in silty soils was also studied before by Cabane (2004). Both studies concluded with conceptual models of silty soils forming aggregates covered by strong lime-treated shells. As a complement, the present research aims at investigating the effect of lime on clayey soils and at characterizing the lime treatment behavior on these types of soils with a complementary conceptual model as well.

Table 1
Properties of the sand and bentonite.

Sand:	
Sibelco© Mol M32	
D_{50} (μm)	260
$C_u = D_{60}/D_{10}$	1.5
ρ_s (g/cm^3)	2.65
Bentonite:	
Ibeco© Deponit CA	
Fine particles (<2 μm)	65%
Silt (2 μm > D > 67 μm)	28%
Sand (>67 μm)	7%
ρ_s (g/cm^3)	2.72
Methylene-blue value (mg/g)	300 ± 30
CEC (meq/100 g)	60 ± 10
Water absorption capacity	≥160%
Free swelling index (ml/2 g)	≥7
Liquid limit	115%
Plastic limit	33%
Plasticity index (calculated)	82%

Table 2
Ingredients for the three different mixtures: the lime quantity is the same and the water content and density follows the MOP curve.

Mixture	10b	15b	20b
Bentonite %	10%	15%	20%
Sand %	90%	85%	80%
Lime %	+1%	+1%	+1%
Water %	+14%	+17%	+20%
ρ_d (g/cm^3)	1.74	1.70	1.64

Mercury Intrusion Porosimetry (MIP) is the second tool selected here to provide a quantitative characterization of the soil microstructure. It was recently applied for lime treatment research. For instance, Cuisinier et al. (2008) used MIP to investigate the effect of alkaline fluid circulation into a sand–bentonite mixture. Le Runigo et al. (2009) studied the microstructure of a lime treated compacted silt submitted to long-term leaching. Combined with suction control, MIP studies were also used in Stoltz et al. (2012) to investigate the effect of swelling and shrinkage on micropores and macropores in lime-treated expansive clayey soils. More recently, Tran et al. (2014) tracked the evolution of the pore size distribution of a lime-treated expansive clay during the first seven days of curing. They observed that macropores (i.e. inter-aggregate pores) increase in size while the intra-aggregate pore-size remains constant. They attribute this change to the hydration of lime that induces a macroscopic swelling. On the contrary, Cuisinier et al. (2013) observed the formation of a small pore population due to lime treatment. Similarly, Russo and Modoni (2013) and Cecconi and Russo (2013) noticed an increase of micropores frequency during curing time on compacted silty soils and pyroclastic soils, respectively, due to the formation of stable bonding compounds that splits large pores into a series of smaller pores. This is consistent with the MIP observations from Metelková et al. (2012) on a compacted and stabilized loess. To study the evolution of the microstructure of lime-treated soils upon wetting–drying cycles, Aldaood et al. (2014) and Khattab et al. (2007), performed MIP tests along curing times after various wetting–drying cycles. They concluded that those hydraulic cycles may have detrimental effects on the soil microstructure but they did not focus on the effect of curing time itself.

In the present study, mixtures of sand and bentonite have been investigated for three different proportions through XRμCT scanning and MIP at different curing times. XRμCT allows obtaining information about the proportion between interparticular macropores and micropores in the bentonite and the local evolution of bentonite due to the presence of lime. The evolution of micro–macro-pores through curing time is also investigated using MIP. Moreover, MIP was used to compare micro–macro-pore proportions with XRμCT measurements.

The paper is structured as follows. Section 2 presents the methodology used for both XRμCT and MIP analyses. The technologies of XRμCT and MIP, the samples preparation, the curing times and the data

Table 3
Summary of the 10 samples scanned under XRμCT. The x markers show the curing times at which the samples were scanned. (*) Accelerated curing at 45 °C after the first 7 days.

	Curing time (days)					
	7	14	17	21	56	105
10b7	x			x*		
15b/7	x		x*			
20b7	x	x*				
10b56					x	
15b56					x	
20b56					x	
10b105						x
15b105						x
20b105						x
15b3t	x	x		x		

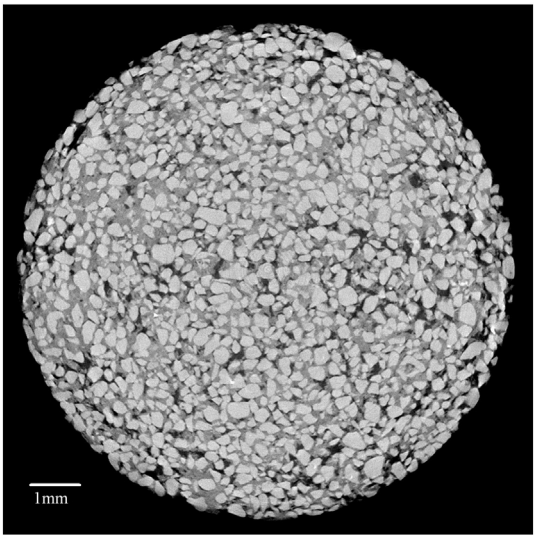

Fig. 1. Cross section of a tomographic image of a lime-treated sand–bentonite mixture.

treatment image registration and segmentation are explained. Afterwards, the results of XRμCT scans are illustrated in Section 3 where the main observations such as a three phase medium interpretation as well as the evolution of soil stabilization during curing are discussed. Then, the observations from the MIP are exposed in Section 4 where the explanations of three porosities are shown together with their evolution in curing. A discussion of these results and their interpretation are given in Section 5 before concluding remarks.

2. Methodology

2.1. Materials composing the mixtures

The effects of the lime treatment of soils can be highly varying from one soil to another as a result of their complex mineral composition. Understanding the behavior of lime treatment is complex and depends on numerous parameters such as: (i) the mineralogy of the involved clays (Carroll, 1959); (ii) interfering materials like organic matter, gypsum, iron minerals, etc. (Netterberg and Paige-Green, 1984; Sherwood, 1993); (iii) the grain shapes and sizes of the skeleton (sand part); (iv) the reactivity of silt and the complexity of its microstructure; and (v) the lime quantity, water content and compaction density (Bell, 1996). The study presented here aims at understanding the microstructure evolution associated with lime treatment avoiding however, in a first approach, the inter-related influence of too many parameters. The presence of any interfering materials will therefore be avoided. To this end, the complex influence of the silt will not be taken into account. The clay will have a single mineralogy and will provide for the clayey cohesive matrix that reacts with lime. The skeleton selected will be chosen as a homometric sand. Based on these assumptions, the model materials studied in this paper are mixtures of sand and bentonite at different proportions. Consequently, this research has the goal to investigate the lime treatment of soils without considering the problem of the diversity of soils from one to another (e.g. the presence of many different clay mineralogies or organic components). The three soils investigated here only differ by their clay and water contents in order to avoid other factors to interfere and render the understanding of the observed effects much more complex.

Moreover, an increasing number of research efforts are focused on the effect of mixing sand and bentonite for different applications, especially for its efficiently low hydraulic conductivity. In the field of study of this paper, lime treated sand–bentonite mixtures can be interesting for their increase in mechanical strength and an alternative to the treatment of sand with cement.

The sand selected for the investigations is homometric (D_{50} = 260 μm and D_{60}/D_{10} = 1.5). The clay matrix is a bentonite which is selected because of its high reactivity with lime (principally montmorillonite) and its wide availability in the market. Calcium bentonite is chosen over sodium bentonite to avoid any excessive swelling upon wetting (free swelling index of 7 ml/2 g following ASTM D5890). It has a 65% weight fraction of fine particles (D < 2 μm), 28% silt (2 μm > D > 67 μm) and 7% sand (D > 67 μm). The lime used is named Proviacal® ST from Lhoist R&D S.A., which is a dry quicklime CL 90-Q in accordance with the norm EN 459-1.

All properties of the sand and bentonite are given in Table 1. The mixtures considered are composed of 10%, 15% and 20% bentonite and respectively 90%, 85% and 80% sand, and are respectively called 10b, 15b and 20b. The lime quantity to be added was calculated according to the Eades and Grim (1966) procedure (ASTM D-6276), and 1% lime was added for all the considered mixtures. The density of the sample

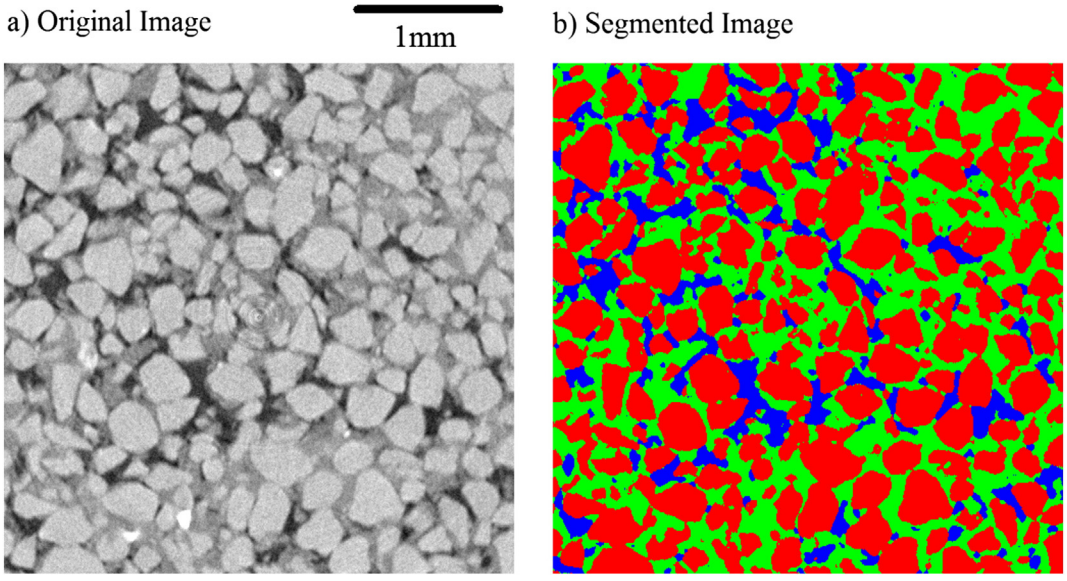

Fig. 2. a) Raw image of a cut in the tomography of one of the mixtures in gray levels; b) image segmentation technique aimed at separating sand (red), bentonite (green) and macrovoid (blue) phases. (For interpretation of the references to color in this figure legend, the reader is referred to the web version of this article.)

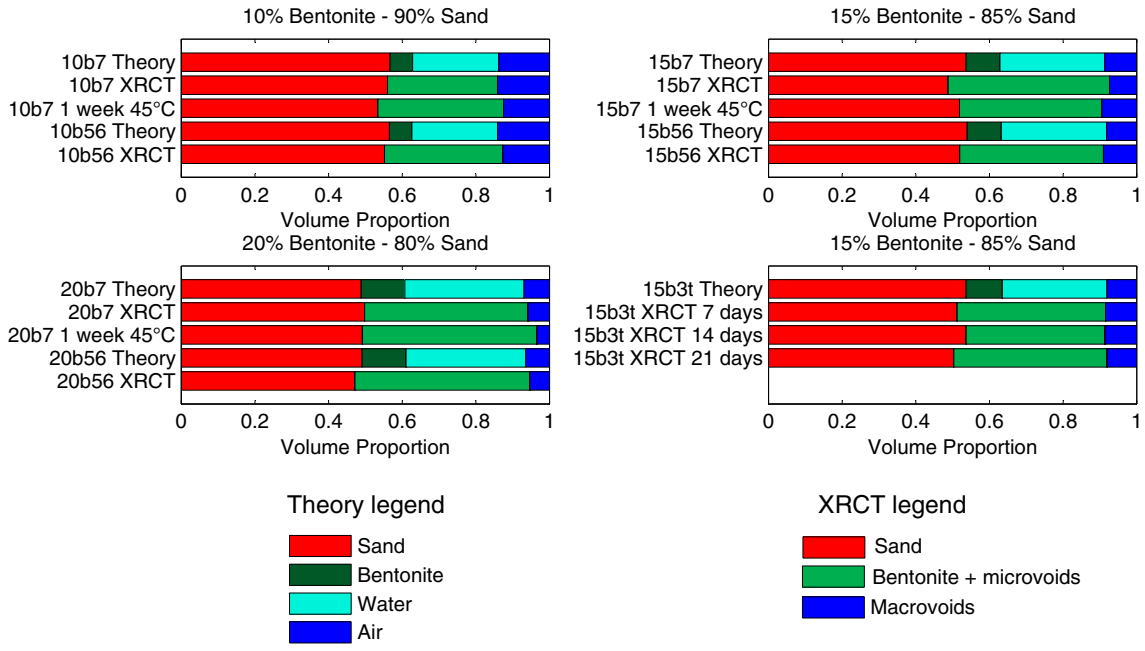

Fig. 3. Comparison between theory and XRμCT images shows that micropores within the bentonite are saturated with water and macropores represent air.

was determined with the Modified Proctor Optimum (MOP) curve of each mixture treated with 1% lime. The compaction was performed according to the Modified Proctor test ASTM D1557. In this procedure, the soil is mixed dry by hand with a precise lime quantity. Distilled water is then poured at different water contents corresponding to the MOP curve of each mixture and the resulting mixture is then mixed by hand. Finally, the wet soil is put in a plastic bag to mellow for 24 h at 20 °C. After 24 h, the samples are compacted at 98.5% of the MOP density. Table 2 summarizes the materials used, the water contents and the densities for preparation of the three mixtures.

2.1.1. Samples for XRμCT

The molds containing the mixtures were made of Plexiglas. The container dimensions were 10 mm height by 10 mm diameter and their precise volume was measured with mercury. The mixtures were introduced in each container with a chemical spatula until the desired weight. The compaction was therefore made statically. All mass measurements were made with an analytical balance with 0.1 mg accuracy. Afterwards, a cap was put on each mold and insulation was achieved with scotch tape followed by paraffin coating. The samples were subsequently stored in a room maintained at 20 °C.

2.1.2. Samples for MIP

Samples of 70 mm height by 36 mm diameter were compacted dynamically, coated with a plastic film and an aluminium foil, sealed with paraffin and, finally, stored at 20 °C for 7 and 56 days. After curing time, the samples were opened and cubic fragments of approximately 1 cm^3 were extracted from their center. The fragments were then freeze-dried and analyzed under MIP.

2.2. X-Ray Micro-Computed Tomography

X-Ray Computed Tomography (X-Ray CT) is a powerful non-invasive technique that allows obtaining a three-dimensional representation of objects. Based on the radiograms of the objects, the computer treatment of the set of images allows obtaining a full three-dimensional gray-level picture representing the local X-Ray attenuation of the material. Used nowadays for a wide variety of applications, this technique was introduced initially for medical imaging (Hounsfield, 1972). The first micro-scale tomography (XRμCT) was performed by Elliot and Dover (1982), with a voxel resolution of 15 μm. An extensive review of the possible use of X-Ray CT can be found in Kalender (2006).

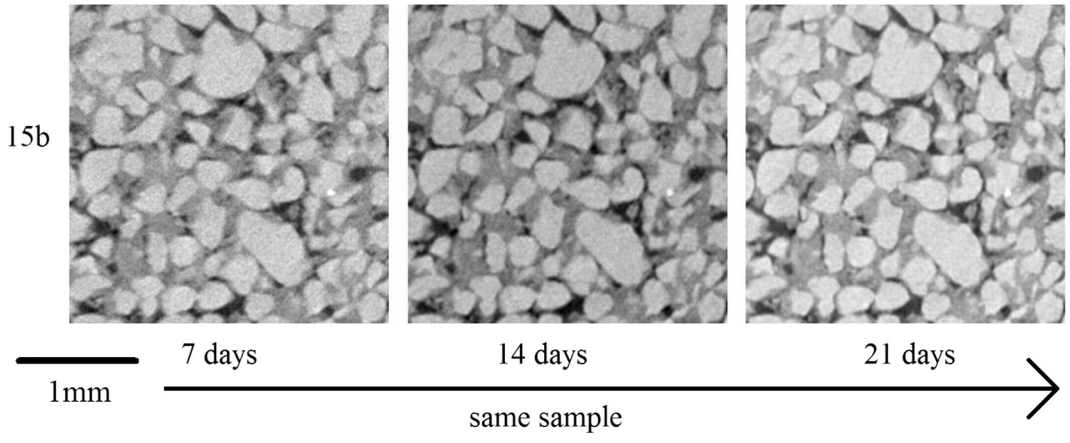

Fig. 4. Images of the same sample of 15b mixture taken at different curing times: images show no visual difference at short curing times.

The resolution of the images taken by the XRμCT is close to 8 μm. This resolution allows characterizing the effects of lime treatment on bentonite at the macroscopic scale (i.e. a few micrometers) relative to the clay particle size which is denoted here the micro-scale. The visual evolution of lime treatment at microscopic (nanometer) clay-scale is not investigated here and could be the topic of future studies (such as Cuisinier et al. (2013), Aldaood et al. (2014) for MIP or Keller et al. (2011) for nanotomography). For XRμCT observation, the concern is to keep the focus on a scale that allows using the classical variables of soil mechanics (porosity and water content, among others). However, MIP, as will be discussed further, is used to explore the micro-scale, which makes the two techniques complementary.

2.2.1. Samples and curing times

The scans presented here were produced in the 3S-R Laboratory of the Université Joseph Fourier in Grenoble, France. The resolution of the images is 7 μm/voxel. To reach such a resolution, cylindrical samples of 10 mm height by 10 mm diameter were used, generating images of 1500 × 1500 × 1500 voxels. In total, 10 samples were prepared. One group of three samples was prepared for scanning after 7 days of curing time (samples 10b7, 15b7 and 20b7). After that, the samples were stored at 45 °C and scanned again after 14 more days for the sample 10b7, 10 more days for the sample 15b7 and 7 more days for the sample 20b7. Curing at 45 °C accelerates the pozzolanic reaction approximately 4–5 times with respect to curing at 20 °C (DeWindt et al., 2014). Consequently, after curing times at 45 °C, the samples 10b7, 15b7 and 20b7

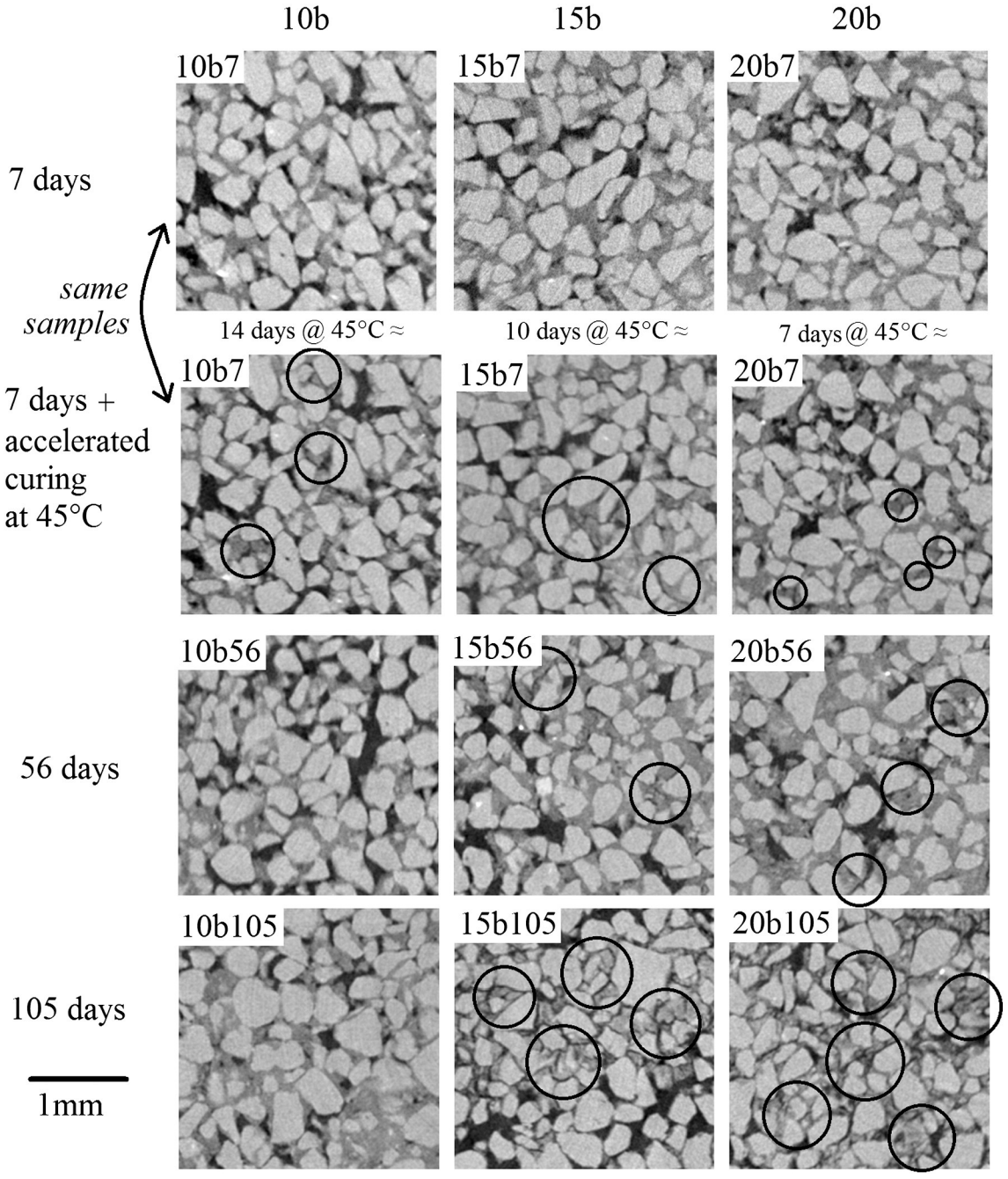

Fig. 5. Images of the three mixtures: 10b, 15b and 20b taken at different long curing times. The two first rows are taken with the same samples while the two last rows are from different samples. Images show cracking appearing in the bentonite phase showing the shrinkage effect of lime on bentonite.

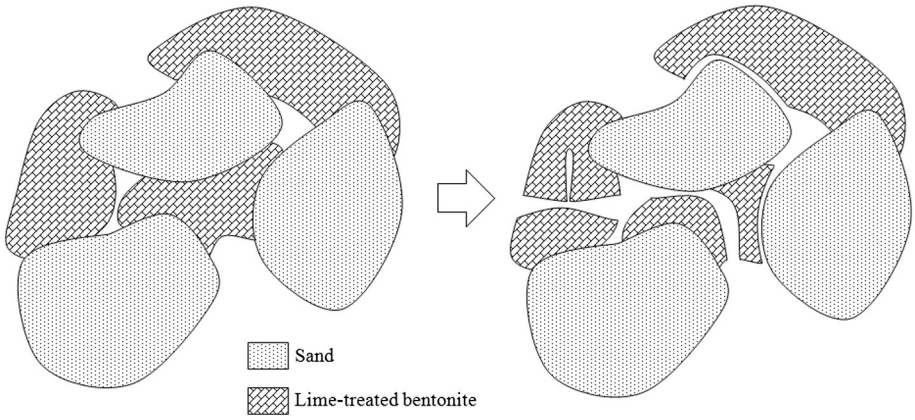

Fig. 6. Conceptual model of bentonite clustering. After a long curing time (more than a few months), the lime-treated bentonite shrinks, cracks and eventually detaches from sand grains.

have an equivalent curing time between one to two months. Two groups of three samples were also prepared to be analyzed at 8 weeks curing time (samples 10b56, 15b56 and 20b56) and 15 weeks curing time (samples 10b105, 15b105 and 20b105). Each group includes the three compositions of the mixtures 10b, 15b and 20b. Finally, a last sample was made from the 15b mixture (sample 15b3t) for analysis at 3 short term curing times: 7 days, 14 days and 21 days. Table 3 summarizes the curing time of all the samples described in this paragraph.

2.2.2. Image segmentation and registration

All tomographic images are composed of three different phases: the sand, the bentonite and the macropores. The micropores cannot be distinguished using this imaging technique because of the tomograph maximum resolution (7 μm/voxel). The gray levels of the three phases are different. However, due to noise and non-homogeneous density (mainly in bentonite), each phase is represented by a Gaussian distribution in the image histogram which induces an overlapping of the gray levels of each of the phases. Moreover, the boundary between the sand phase (high gray level) and the macrovoid phase (low gray level) has the same gray level as the bentonite phase (middle gray level) due to Partial Volume Effects, a common artifact in XRCT imaging explained for example in Mukunoki et al. (2004). Therefore, a simple threshold technique could not deliver a proper segmentation of the three phases, and the segmentation methodology developed in Hashemi et al. (2014) was used.

To investigate the evolution of a given sample as a function of time, the numerical difference of gray levels between two images at two different times can be used. However, when a sample is scanned several times (to evaluate the evolution of the soil microstructure during curing), it is not positioned identically at every scan. Hence, the tomographic images do not perfectly match and an image registration should be used. For more information about image registration, the reader can refer to Zitova and Flusser (2003). The image registration involves an affine transformation

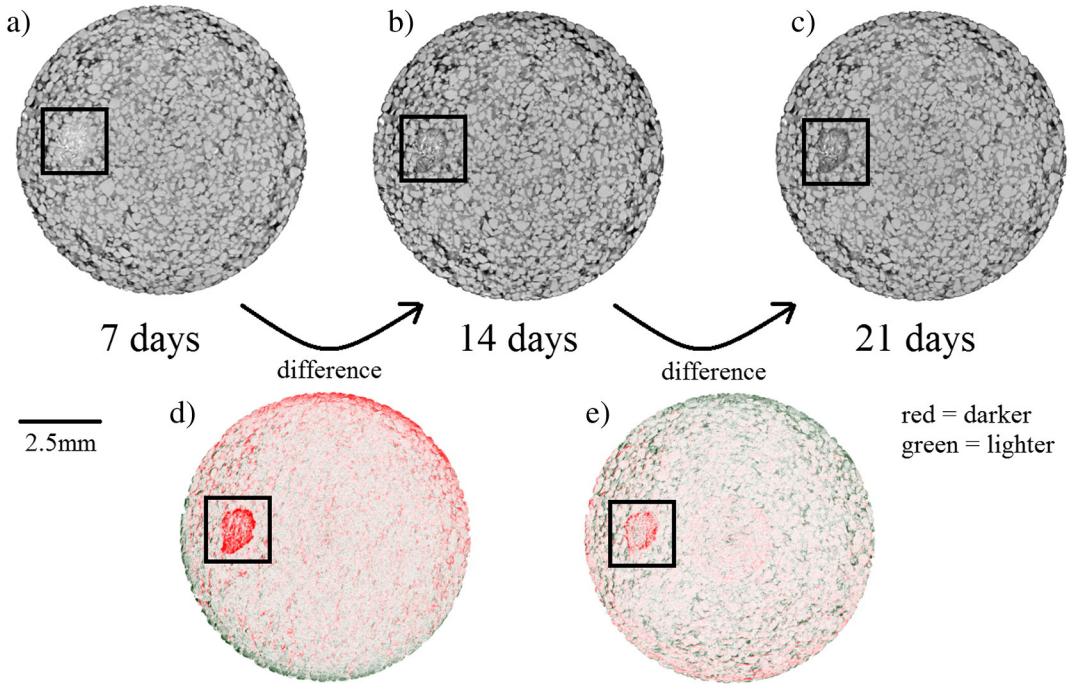

Fig. 7. Difference of gray levels makes evolution detection easier: red shows evolution into darker gray values and green into clearer. Sample 15b3t at a) 7 days, b) 14 days, c) 21 days; d) difference between a) and b); e) difference between b) and c). The square represents the zone zoomed in Fig. 8. (For interpretation of the references to color in this figure legend, the reader is referred to the web version of this article.)

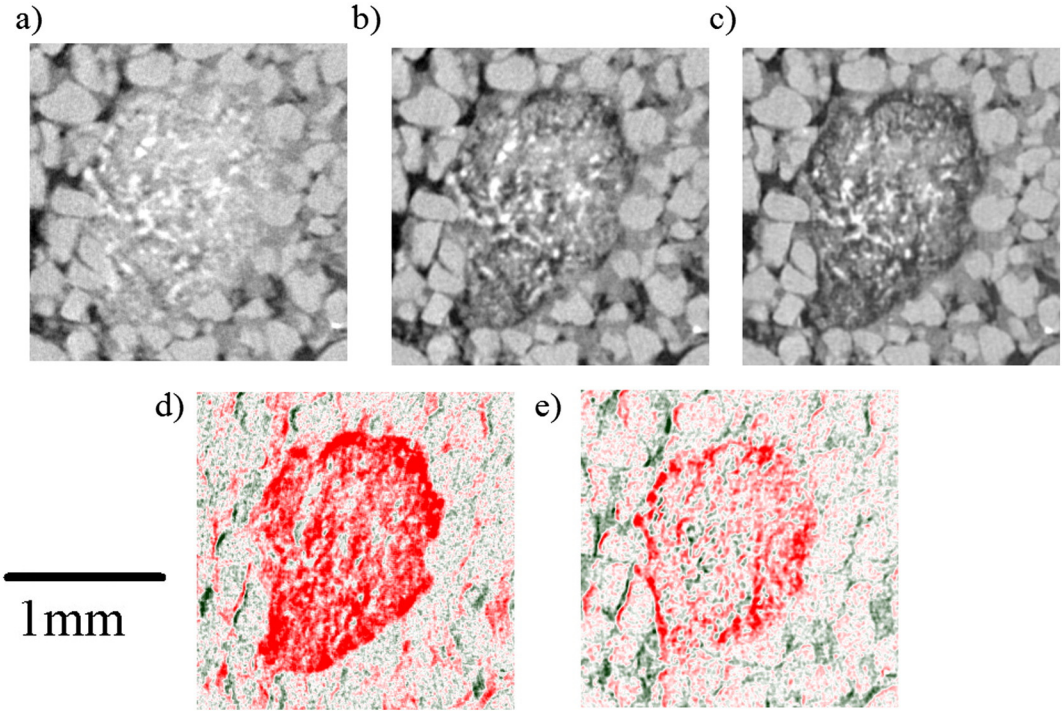

Fig. 8. Detail of the sample presented in Fig. 7 showing the cluster of highly enriched lime region. (For interpretation of the references to color in this figure legend, the reader is referred to the web version of this article.)

(as proposed in Gentle (2007)) followed by a contrast matching. The affine transformation 4 × 4 matrix R transforms a set of coordinates into another according to:

$$(x_i \quad y_i \quad z_i \quad 1)R = (x_i' \quad y_i' \quad z_i' \quad 1). \tag{1}$$

However, to calculate first the R matrix, at least 4 matching points from both images have to be selected. Lime particles in the samples are good candidates for this purpose as their high gray level makes them easily selectable with a simple threshold on the histogram, and as their location is completely dispersed throughout the sample. An arbitrary threshold is made to select the highest gray level voxels. Around 15,000 are selected in both images. The voxels appear in clusters representing the lime particles. The same clusters appearing on both images are then manually selected. The center of each cluster is put as coordinates in Eq. (1) as (x_i, y_i, z_i) for the first image and (x_i', y_i', z_i') for the second image. 8 coordinates for each image were chosen in order to obtain a more accurate value of R calculated therefore by the least-squares method.

2.3. Mercury Intrusion Porosimetry

MIP is an effective tool to analyze the fabric of porous media that was first noticed by Washburn (1921). Using the non-wetting property of mercury, the pressure required to force mercury into a porous medium is inversely proportional to the entrance radius of its pores according to:

$$p = -\frac{2\gamma\cos\theta}{r} \tag{2}$$

where p is the capillary pressure, γ is the surface tension of mercury (0.485 N/m), θ is the contact angle between mercury and solids (130°) and r is the entrance radius of the pore. The cumulative intrusion of the soil is determined by gradually increasing the pressure of mercury intrusion into the soil and determining the volume entrance for each pressure. The derivative of the cumulative intrusion with respect to the logarithm of the pore size yields the incremental intrusion which represents the pore size distribution (PSD) of the soil. However, it should be noticed that this method does not take isolated pores into account and suffers from the ink-bottle effect as it may count some pores as a smaller size if they are located behind bottlenecks (thus

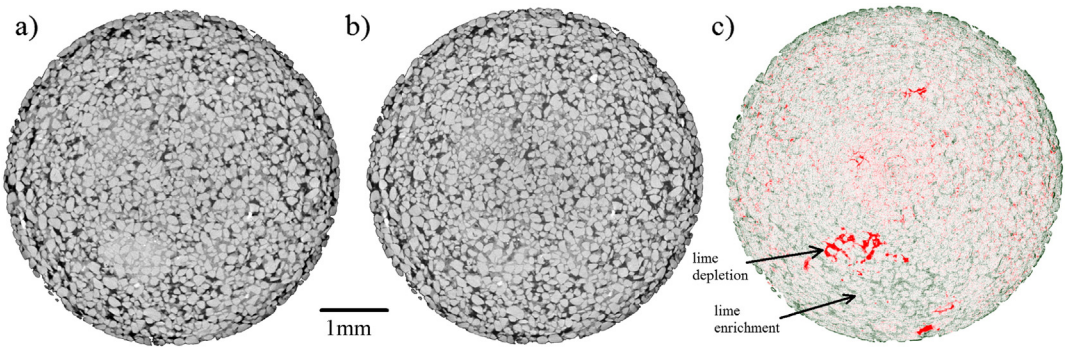

Fig. 9. a) A cross section of the 10b7 sample at 7 days curing time showing a region rich in lime; b) the same cross section after 7 days at 45 °C; c) difference between the two images (red = decrease of gray value, green = increase of gray value). (For interpretation of the references to color in this figure legend, the reader is referred to the web version of this article.)

underestimating the cumulative pore size distribution). Romero and Simms (2008) presented a wide review about the use of MIP in geomaterials, showing the efficiency of MIP in spite of the above mentioned limitation.

The MIP was performed in Lhoist R&D Laboratory using the device Micromeritics AutoPore IV 9500. Pressures of intrusion range from 3.5 kPa to 200 MPa, corresponding to filling pores from 350 μm down to 6 nm.

3. Results of XRμCT

3.1. Three phase medium and image segmentation

In this study, a distinction will be made between the phases (as observed from XRμCT) and the constituents (corresponding to raw materials). As illustrated in Fig. 1, the samples are composed of three phase: the sand, the bentonite–lime mixture and the macropores. Lime particles can also be seen from place to place in pure white. The raw materials are made of four constituents (sand, bentonite, air, water). The lime volume and mass were neglected due to the low proportion present in the mixture. The segmentation of these images was performed (see Hashemi et al. (2014)) in the phases mentioned above as shown in Fig. 2, where Fig. 2a is the original image and Fig. 2b is the segmented image. Based on the segmentation of the images representing the three mixtures, it is possible to estimate volume proportions of each phase in the samples. Consequently, knowing the total porosity of the sample from macroscopic data and the macroporosity from XRμCT, the proportion between micropores and macropores can be calculated as well as the mean dry density of the bentonite aggregates located between the sand particles. These phase proportions are depicted for comparison with the volume of each constituent of the mixture in Fig. 3. The volume proportions of each constituent of the mixture were calculated by determining its mass in the mixture and its specific density. Measurements of specific density for sand and bentonite were performed using the pycnometer whereas the water was supposed to have a density of 1. Specific densities of sand and bentonite are shown in Table 1. The results show that the volume of the macropores phase is equivalent to the air volume while the volume of the bentonite phase is equal to the sum of the volume of water and bentonite constituents. In other words, this means that the bentonite absorbs all the water contained in the mixture and becomes saturated. The micro–macro-distribution of pores in the sand–bentonite mixtures is consequently controlled by macroscopic parameters: the water content w, the dry density ρ_d, the specific density of sand $\rho_{s,s}$, the specific density of bentonite $\rho_{s,b}$ and the mass proportion of bentonite in the sand–bentonite mixture b (here 10%, 15% or 20%). The total porosity is given by

$$n = 1-\rho_d\left(\frac{1-b}{\rho_{s,s}}+\frac{b}{\rho_{s,b}}\right) \tag{3}$$

while the microporosity n_μ and macroporosity n_M are given by:

$$n_\mu = w\frac{\rho}{\rho_w}, n_M = n-n_\mu \tag{4}$$

where ρ_w is the density of water and ρ is the bulk density. Finally, the dry density $\rho_{d,b}$ of the bentonite phase in the mixture is given by:

$$\frac{1}{\rho_{d,b}} = \frac{1}{\rho_{s,b}}+\frac{w}{b\rho_w}. \tag{5}$$

3.2. Microstructural evolution of bentonite

As explained in Section 2.2.1, samples of three different mixtures were analyzed at different curing times. Fig. 4 shows the same zone obtained from one sample scanned at 7 days, 14 days and 21 days curing times. From these three images, it can be concluded that no important visual difference can be identified at short curing time. Conversely, Fig. 5 illustrates the effects of longer curing times and shows evidence

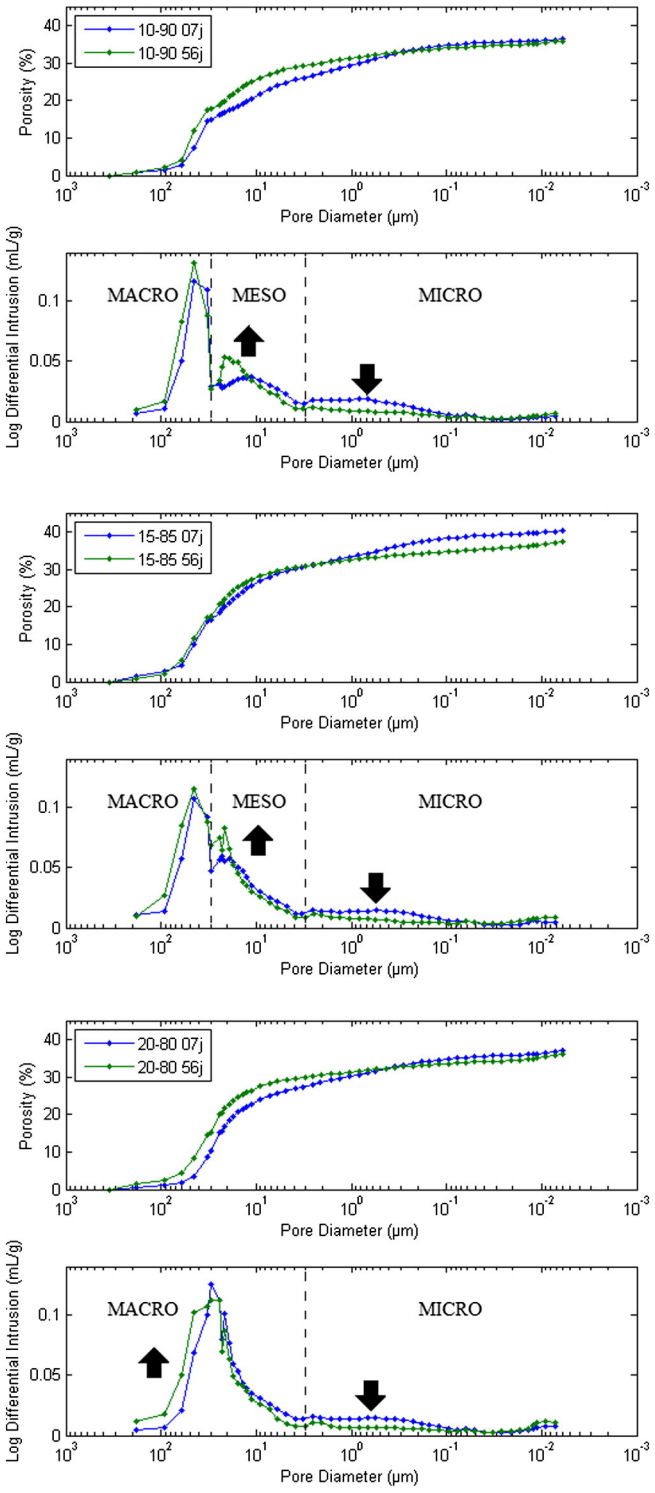

Fig. 10. Cumulative porosity and pore size distribution of the three mixtures at 7 and 56 days of curing time.

of changes in the bentonite phase. Due to the shrinking of the bentonite phase with the effect of lime, some cracks appear for the samples 15b56, 15b105, 20b56 and 20b105. They also appear at longer curing times (105 days) in the sample 10b105 and in the sample subjected to accelerated curing times. During pozzolanic reaction, lime consumes a part of the water from the bentonite, thereby inducing shrinkage. Due to the peculiar bi-modal microstructure of this sand–bentonite mixture, the sand skeleton particles provide stiffness against macroscopic shrinkage. However, at microscale, bentonite tends to shrink. This shrinkage is constrained by the rigid sand skeleton which induces the appearance of tensile cracks in bentonite. This effect is amplified by the fact that the plastic limit of bentonite is significantly reduced by the lime treatment. The lime reaction reduces the ductility of the bentonite which cannot accommodate the deformation induced by shrinkage, hence leading to tensile cracks. It is noted that this cracking phenomenon may be specific to this particular bi-modal microstructure and generalization to all types of soils remains to observe. At 105 days, it appears that the cracks in the bentonite phase of the 15b and 20b mixtures are numerous, corresponding to an advanced state of the reaction. Fig. 6 depicts a conceptual model of this effect. The visualization under XRμCT of lime treated sand–bentonite mixtures shows that the bentonite phase shrinks and forms hard clusters around the sand grains and interlocks. Cracks are formed in the bentonite phase and, eventually, between the bentonite itself and the surrounding sand grains.

3.3. Lime migration

The evolution of the soil microstructure of the same sample at different curing times can be characterized by determining the difference between the corresponding images. This is illustrated, for the sample 15b3t scanned under XRμCT at three curing times (7, 14 and 21 days), in Figs. 7 and 8, where such a gray level difference is used to detect evolution. Fig. 7d and e depicts the difference between the 7 days and the 14 days curing times and between 14 days and 21 days curing times, respectively. Red pixels show a decreasing gray value while green pixels show an increasing value. The cross section in the figure was explicitly chosen to show a cluster of highly lime-enriched regions in the sample. The detail of this cluster is shown in Fig. 8. The pictures show a migration of a phase in middle gray value around the cluster. The gray level of this phase is slightly clearer with respect to the bentonite phase gray level. It is here postulated that this is a “lime-enriched aggregate”. The aggregate occupies first the macropores and is progressively absorbed by the bentonite phase. The detail in Fig. 8 shows, between the first and the second weeks of curing, a global change in the gray level whereas, between the second and the third weeks, the change is rather located on the edge of the aggregate. It is however not trivial to differentiate the lime-enriched aggregate from the bentonite phase in the XRμCT images as they both have close X-Ray absorptivities. This effect is observed in few parts of different samples. Fig. 9 shows the same effect of lime migration at a broader scale for the 10b7 sample scanned twice. The presence of a higher macroporosity in a 10b mixture than in the two others suggests the existence of lime-enriched aggregate formation. The red zone in Fig. 9c is closely surrounded by a more disperse green zone suggesting that lime migrated into the bentonite phase.

The effect of lime migration is less or not present in the two other scanned samples 15b7 and 20b7 as it may be highly dependent on the process of soil mixing and the homogeneity of the mixture as well as on the higher macroporosity availability in the 10b mixture. An area with high lime concentration exists between sand particles and bentonite aggregates. After a few weeks, the lime migrates into the surrounding bentonite and leaves either a void or a less lime-concentrated area at the starting point. This model is close to the conceptual model already shown in literature by Locat et al. (1990), where the aggregates of lime diffuse through water and surround the clay particles, thereby increasing their strength.

4. Results of MIP

Six samples have been analyzed for MIP representing the three mixtures 10b, 15b and 20b multiplied by two curing times, at 7 days and 56 days. The evolution of the distribution of pore size measured with MIP is consistent with the vizualization under XRμCT. Fig. 10 presents for the three mixtures, the results of the MIP on samples at 7 days and 56 days of curing times. According to the pore size distribution of every sample, three categories of pores can be defined: micropores for $D < 3$ μm, mesopores for D included between 3 μm and 30 μm and macropores larger than 30 μm. Those limits correspond to the minima of pore size distribution curve obtained and are not related to any standard of pore size separation. In particular, the IUPAC classification, extensively used in clay sciences, considering the processes occurring at nanoscale, is clearly not our scale of interest and cannot be used in the present study. Consequently, a specific separation of pore size has been defined, consistent with the multi-modal pore-size distribution observed. For all three mixtures, it is observed that the fraction of micropores decreases with curing time. On the other hand, the total porosity remaining constant, pores larger than 3 μm increase in volume. For the mixtures 10b and 15b, the porosity above 3 μm is a combination of mesopores and macropores. Both mesopores and macropores in both mixtures 10b and 15b increase in size during curing. The peak of the mesopores distribution in 10b7 is growing from 10 μm to 20 μm, while in the 15b mixture, the increase of the mesopores size is lower but their volume fraction increases. The mixture 20b has only one class of porosity above 3 μm because the minimum at 30 μm is not clearly visible. For high bentonite content (20b samples), the characteristic size of macropores is slightly lower than for 10b and 15b samples. This is due to the fact that bentonite better fills the space between sand grains. As a consequence, macropores and mesopores are merged, which explains why the mesopores are not explicitly visible in the MIP of 20b samples. The macroporosity in the mixture 20b increases with curing time as in the case of the mesopores in the mixtures 10b and 15b. Fig. 11 shows a conceptual model of this evolution.

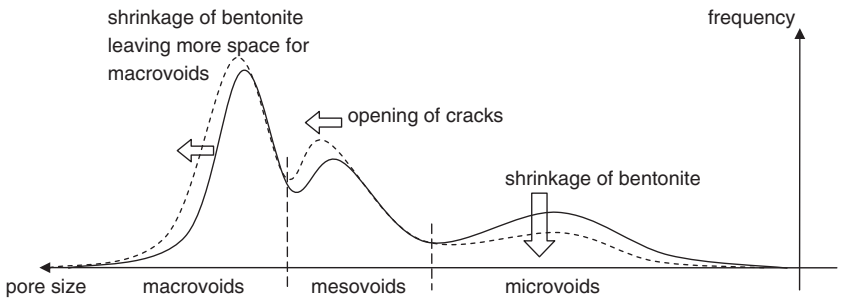

Fig. 11. Conceptual model of the microstructure fabric evolution with curing time. The model shows a division in three categories evolving differently.

5. Discussion

In Section 3.1, it was found that the proportions between micro- and macro-pores can be calculated theoretically by assuming that bentonite is fully saturated while macrovoids are full of air. The total porosity of the samples matches this theoretical estimation (which is between 35% and 40%). As explained in the previous section, the micropores considered in MIP are those with an equivalent diameter smaller than 3 μm. The mesopores and macropores of MIP results (pores larger than 3 μm) will be denoted, in this paragraph, as macropores. Table 4 shows the proportions of micro- and macropores obtained by means of the MIP results. Even if the general trend is consistent between MIP and XRμCT, it can be seen that MIP overestimates the amount of macropores and underestimates the micropores. The most plausible explanation is as follows. Once the sand–bentonite mixture is freeze-dried, the structure and organization of the clay particles remain unchanged. However, this clay structure without water is made much more brittle and its fabric can be easily damaged. This leads to the fact that intruding the mercury will inevitably widen the macropores by compacting the clay aggregates. This is the case when mercury fills the macrovoids while microvoids are still empty. The transition of mercury from macropores to micropores ranges from 30 μm to 3 μm. These diameters correspond to mercury intruding at pressures from 0.4 bar to 4 bars which is enough to modify the clay structure. Consequently, the intrusion of mercury may affect the structure of the clay particles. It widens the macropores and compacts the clay aggregates thus decreasing micropores. However, in total, the porosity remains the same as theoretically expected.

Even though the proportion between macropores and micropores cannot be quantitatively described with MIP, the evolution of lime treatment on the mixture porosity is clearly shown. Moreover, a similarity can be seen when combining XRμCT and MIP. The decrease of proportions of micropores between 7 days and 56 days of curing times, observed in MIP, is consistent with the visual observation of bentonite shrinkage in XRμCT. The presence of cracking and bentonite shrinking in XRμCT can be translated to the increase in size or volume of macropores in the MIP. In Fig. 5, at 56 days, the samples 15b56 and 20b56 exhibit cracking. These cracks are 1 to 2 voxels wide which approximately corresponds to an order of magnitude of 10 μm (the resolution of the picture is 7 μm/voxel). By looking in the MIP results, the increase of macropores during curing is a consequence of the bentonite shrinkage that opens cracks of the order of 10 μm.

6. Conclusions

In order to provide a microstructural interpretation of the macroscopic evidence of soil stabilization with lime, this study had the objective to investigate the micro-scale using XRμCT (at the scale of 10 to 100 μm) and MIP (between 10 nm to 100 μm). Controlled mixtures of sand and bentonite were tested at three different proportions: 10%, 15% and 20% of bentonite and 90%, 85% and 80% of sand with added water content of, respectively, 14%, 17% and 20% of total weight (corresponding to Modified Optimum Proctor water content). All mixtures were treated with 1% of lime and then compacted at 98.5% of Modified Optimum Proctor dry density. Samples for XRμCT were created for the three mixtures at different curing times (7, 14, 21, 56 and 105 days). Samples for MIP were created for the three main mixtures at 7 days and 56 days curing times. The obtained results allow drawing the following conclusions:

1. The relative proportion between micropores and macropores is governed only by macroscopic parameters: the water content, the bulk density, the specific density of sand and the specific density of bentonite. Micropores are concentrated in the bentonite aggregates and are filled exclusively with water. Macropores, on the other hand, are inter-aggregate pores between sand particles and bentonite aggregates and are exclusively full of air.
2. XRμCT scans of a given sample at different curing times show on some samples the migration of lime throughout the mixture. These migrations are detectable by image registration and image differentiation. The evolution of lime-enriched aggregates is such that the quantity of lime in these aggregates decreases and migrates in the surrounding bentonite.
3. Once bentonite is reacting with lime, after a given period (2–4 months), the bentonite aggregates shrink and crack. This in turn causes an increase of the macroporosity and a decrease of the microporosity. MIP results are reliable to show this evolution qualitatively. The amplitude of this cracking phenomenon of bentonite is potentially linked to the peculiar bi-modal microstructure of the sand–bentonite mixture. The sand skeleton provides a significant stiffness that avoids macroscopic shrinkage while bentonite shrinks due to the lime reaction. This differential shrinkage behavior between skeleton and bentonite induces cracking.

Table 4
Proportions of micropores and macropores in MIP show a significant difference from theory (valid with XRμCT). However total porosity is comparable in both measurement methods.

Mixture	Micro *n* (%)	Macro *n* (%)	Total *n* (%)
10b (theory)	23.1%	12.4%	35.5%
10b (MIP 7d)	10.2%	26.1%	36.3%
10b (MIP 56d)	16.4%	29.3%	35.7%
15b (theory)	27.5%	10.0%	37.5%
15b (MIP 7d)	9.6%	30.7%	40.3%
15b (MIP 56d)	6.4%	30.8%	37.2%
20b (theory)	32.5%	5.7%	38.2%
20b (MIP 7d)	9.4%	27.5%	36.9%
20b (MIP 56d)	6.2%	29.8%	36.0%

Acknowledgments

The support from F.R.S–FNRS Belgium for experimental equipments through grant 2.4.626.10.F is gratefully acknowledged.

References

Aldaood, A., Bouasker, M., Al-Mukhtar, M., 2014. Impact of wetting drying cycles on the microstructure and mechanical properties of lime-stabilized gypseous soils. Eng. Geol. 174, 11–21.
Al-Mukhtar, M., Khattab, S., Alcover, J., 2012. Microstructure and geotechnical properties of lime-treated expansive clayey soil. Eng. Geol. 139–140, 17–27.
Anderson, S.H., Gantzer, C.J., Boone, J.M., 1988. Rapid non destructive bulk density and soil water content determination by computed tomography. Soil Sci. Soc. Am. J. 52, 35–40.
Arabi, M., Wild, S., Rowlands, G., 1989. Frost resistance of lime-stabilized clay soil. Transp. Res. Rec. 1219, 93–102.
Bell, F.G., 1996. Lime stabilization of clay minerals and soils. Eng. Geol. 42, 223–237.
Cabane, N., 2004. Sols traités à la chaux et aux liants hydrauliques: Contribution à l'identification et à l'analyse des éléments perturbateurs de la stabilisation. Ph.D. thesis. Ecole Nationale Supérieure des Mines de Saint-Etienne.
Carroll, D., 1959. Ion exchange in clays and other minerals. Geol. Soc. Am. Bull. 70 (6), 749–779.
Cecconi, M., Russo, G., 2013. Microstructural features of lime-stabilised pyroclastic soils. Géotech. Lett. 3, 124–129.
Cuisinier, O., Masrouri, F., Pelletier, M., Villieras, F., Mosser-Ruck, R., 2008. Microstructure of a compacted soil submitted to an alkaline plume. Appl. Clay Sci. 40, 159–170.
Cuisinier, O., Auriol, J.C., Le Borgne, T., Deneele, D., 2013. Microstructure and hydraulic conductivity of a compacted lime-treated soil. Eng. Geol. 123, 187–193.
De Bel, R., Gomes Correia, A., Verbrugge, J.-C., 2009. Contribution of loamy soil treatment to improve embankments performance. Geotech. Spec. Publ. ASCE 189, 61–72.
Desrues, J., Chambon, R., Mokni, M., Mazerolle, F., 1996. Void ratio evaluation inside shear bands in triaxial sand specimens studied by computer tomography. Geotechnique 3 (46), 529–546.
Desrues, J., Viggiani, G., Besuelle, P., 2006. Advances in X-ray tomography for geomaterials. iSTE, London, UK.
DeWindt, L., Deneele, D., Maubec, N., 2014. Kinetics of lime/bentonite pozzolanic reactions at 20 and 50 °C: batch tests and modeling. Cem. Concr. Res. 59, 34–42.
Diamond, S., Kinter, E.B., 1965. Mechanisms of soil–lime stabilization. Highw. Res. Rec. 92, 83–102.

Eades, J.L., Grim, R.E., 1966. A quick test to determine lime requirements for lime stabilization. Highw. Res. Rec. 139, 61–72.
Eades, J.L., Nichols, F.P., Grim, R.E., 1962. Formation of new minerals with lime stabilization as proven by field experiments in Virginia. Highw. Res. Board Bull. 335, 31–39.
Elliot, J.C., Dover, S.D., 1982. X-ray microtomography. J. Microsc. 126 (2), 211–213.
Gentle, J., 2007. Matrix algebra: theory, computations, and applications in statistics. Springer Science & Business Media.
Hall, S.A., Bornert, M., Desrues, J., Pannier, Y., Lenoir, N., Viggiani, G., Bésuelle, P., 2010. Discrete and continuum analysis of localised deformation in sand using X-ray μCT and volumetric data image correlation. Geotechnique 60 (5), 315–322.
Hashemi, M.A., Khaddour, G., François, B., Massart, T.J., Salager, S., 2014. A tomographic imagery segmentation methodology for multi-phase granular materials based on simultaneous region growing. Acta Geotech. 9, 831–846.
Higo, Y., Oka, F., Kimoto, S., Sanagawa, T., Matsushima, Y., 2011. Study of strain localization and microstructural changes in partially saturated sand during triaxial tests using microfocus X-Ray CT. Soils Found. Jpn. Geotech. Soc. 51 (1), 95–111.
Hounsfield, G. N., 1972. Apparatus for examining a body by radiation such as X or gamma radiation. British Patent No 1.283.915, London.
Kalender, W.A., 2006. X-ray computed tomography. Institute of physics publishing. Phys. Med. Biol. 51, R29–R43.
Kawaragi, C., Yoneda, T., Sato, T., Kaneko, K., 2009. Microstructure of saturated bentonites characterized by X-ray CT observations. Eng. Geol. 106 (1/2), 51–57.
Keller, W.D., 1964. Process of origin and alteration of clay mineral, soil clay mineralogy. In: Rich, C.I., Kunze, G.W. (Eds.), University of North Carolina.
Keller, L.M., Holzer, L., Wepf, R., Gasser, P., 2011. 3d geometry and topology of pore pathways in Opalinus clay: implications for mass transport. Appl. Clay Sci. 52, 85–95.
Ketcham, R.A., Carlson, W.D., 2011. Acquisition, optimization and interpretation of X-ray computed tomographic imagery: applications to geosciences. Comput. Geosci. 27, 381–400.
Khattab, S.A.A., Al-Mukhtar, M., Fleureau, J.M., 2007. Long-term stability characteristics of a lime-treated plastic soil. J. Mater. Civ. Eng. 19, 358–366.
Le Runigo, B., Cuisinier, O., Cui, Y.-J., Deneele, D., Ferber, V., 2009. Impact of the initial state on fabric and permeability of a lime treated silt under long term leaching. Can. Geotech. J. 46 (11), 12431257.
Lemaire, K., Deneele, D., Bonnet, S., Legret, M., 2013. Effects of lime and cement treatment on the physicochemical, microstructural and mechanical characteristics of a plastic silt. Eng. Geol. 166, 255–261.
Lenoir, N., Bornert, M., Desrues, J., Bésuelle, P., Viggiani, G., 2007. Volumetric digital image correlation applied to X-Ray microtomography images from triaxial compression tests on argillaceous rocks. Strain Int. J. Exp. Mech. 43 (3), 193–205.
Little, D.N., 1964. Handbook for stabilization of pavement subgrades and base courses with lime. Kendall and Hunt, University of North Carolina.
Locat, J., Bérubé, M.A., Choquette, M., 1990. Laboratory investigations on the lime stabilization of sensitive clays: shear strength development. Can. Geotech. J. 27, 294–304.
Mees, F., Swennen, R., Van Geet, M., Jacobs, P., 2003. Applications of X-ray computed tomography in the geosciences. Geol. Soc. Lond. Spec. Publ. 215, 1–6.
Metelková, Z., Boháč, J., Přikryl, R., Sedlářová, I., 2012. Maturation of loess treated with variable lime admixture: pore space textural evolution and related phase changes. Appl. Clay Sci. 61, 37–43.
Mukunoki, T., Otani, J., Obara, Y., Kaneko, K., 2004. Artifacts of X-Ray CT data in the analysis of geomaterial properties. In: Otani, Obara (Ed.), X-ray CT for Geomaterials; Soils, Concrete, Rocks. Swets and Zeitlinger, Lisse, pp. 95–101.
Netterberg, F., Paige-Green, P., 1984. Carbonation of lime and cement stabilized layers in road construction. Tech. Rep. National Institute for Transport and Road Research, CSIR, South-Africa.
Riedel, I., Ando, E., Salager, S., Bésuelle, P., Viggiani, G., 2012. Water retention behaviour explored by X-ray CT analysis. Proceedings of 2nd European Conference on Unsaturated Soils, pp. 81–88.
Romero, E., Simms, P.H., 2008. Microstructure investigation in unsaturated soils: a review with special attention to contribution of mercury intrusion porosimetry and environmental scanning electron microscopy. Geotech. Geol. Eng. 26 (6), 705727.
Russo, G., Modoni, G., 2013. Fabric changes induced by lime addition on a compacted alluvial soil. Géotech. Lett. 3, 93–97.
Saba, S., Barnichon, J.D., Cui, Y.-J., Tang, A.M., Delage, P., 2014. Microstructure and anisotropic swelling behaviour of compacted bentonite/sand mixture. J. Rock Mech. Geotech. Eng. http://dx.doi.org/10.1016/j.jrmge.2014.01.006.
Sherwood, P., 1993. Soil stabilization with cement and lime. State of the art review. Tech. Rep. Transport Research Laboratory, HMSO, London.
Stoltz, G., Cuisinier, O., Masrouri, F., 2012. Multi-scale analysis of the swelling and shrinkage of a lime-treated expansive clayey soil. Appl. Clay Sci. 61, 44–51.
Taud, H., Martinez-Angeles, R., Parrot, J.F., Hernandez-Escobedo, L., 2005. Porosity estimation method by X-ray computed tomography. J. Pet. Sci. Eng. 3–4 (47), 209–217.
Thompson, M.R., 1965. Shear strength and elastic properties of lime–soil mixtures. University of Illinois, Urbana, Ill.
Tran, T.D., Cui, Y.-J., Tang, A.M., Audigier, M., Cojean, R., 2014. Effects of lime treatment on the microstructure and hydraulic conductivity of Héricourt clay. J. Rock Mech. Geotech. Eng. 6, 399–404.
Washburn, E.W., 1921. Note on a method of determining the distribution of pore sizes in a porous material. Proc. Natl. Acad. Sci. U. S. A. 7 (4), 115116.
Zitova, B., Flusser, J., 2003. Image registration methods: a survey. Image Vis. Comput. 21 (11), 977–1000.